tvst

Article

Imaging of Age-Related Macular Degeneration by Adaptive Optics Scanning Laser Ophthalmoscopy in Eyes With Aged Lenses or Intraocular Lenses

Yuhua Zhang[1,2], Xiaolin Wang[2], Mark E. Clark[3], Christine A. Curcio[3,*], and Cynthia Owsley[3,*]

[1] Department of Ophthalmology, University of California–Los Angeles, Los Angeles, CA, USA
[2] Doheny Eye Institute, Los Angeles, CA, USA
[3] Department of Ophthalmology and Visual Sciences, University of Alabama at Birmingham, Birmingham, AL, USA

Correspondence: Yuhua Zhang, PhD, Doheny Eye Institute, Department of Ophthalmology, University of California–Los Angeles, 1355 San Pablo Street, Los Angeles, CA 90033, USA. e-mail: yzhang@doheny.org

Received: January 15, 2020
Accepted: June 12, 2020
Published: July 29, 2020

Keywords: adaptive optics scanning laser ophthalmoscopy; lens opacity; cataract; retina; photoreceptors

Citation: Zhang Y, Wang X, Clark ME, Curcio CA, Owsley C. Imaging of age-related macular degeneration by adaptive optics scanning laser ophthalmoscopy in eyes with aged lenses or intraocular lenses. Trans Vis Sci Tech. 2020;9(8):41, https://doi.org/10.1167/tvst.9.8.41

Purpose: To assess the performance of adaptive optics scanning laser ophthalmoscopy (AOSLO) in a large sample of eyes with or without age-related macular degeneration (AMD) and with cataracts or intraocular lenses (IOLs).

Methods: Patients with various degrees of AMD and age-similar normal subjects underwent fundus photography. Cataract severity and IOL clarity were assessed by fundus reflex photographs. In phakic eyes, lenticular opacity was graded as nuclear, cortical, or posterior subcapsular cataract. In eyes with IOLs, lens clarity was assessed by posterior capsule opacification (PCO). Quality of AOSLO images of the macular photoreceptor mosaic was classified as good, adequate or inadequate by human graders in a subjective assessment of cone visibility.

Results: A total of 159 eyes in 80 subjects (41 males, 39 females, aged 72.5 ± 11.5 years, 16 normals) were examined. Seventy-nine eyes had IOLs, and 80 eyes were phakic. AOSLO produced good images in 91 eyes (57%), adequate images in eight eyes (5%), and inadequate images in 27 eyes (17%). AOSLO did not acquire images in 33 eyes (21%), because of dense lenticular opacity, widespread PCO, or problems specific to individual subjects.

Conclusions: AOSLO images considered at least Adequate or better for visualizing cone photoreceptors were acquired from 62% of study eyes.

Translational Relevance: AOSLO can be used as an additional imaging modality to investigate the structure of cone photoreceptors in research on visual function in AMD and in clinical trials involving older patients.

Introduction

Adaptive optics scanning laser ophthalmoscopy (AOSLO)[1] has been demonstrated as an important high-resolution imaging modality for studying photoreceptor morphology in healthy and diseased eyes thereby elucidating mechanisms of photoreceptor degeneration and loss.[2–4] It has been developed with confocal imaging mode[1] and nonconfocal mode.[5–7] Cones are reliably imaged by both modalities,[2,4] whereas rods have been imaged by confocal AOSLO only in healthy eyes or in eyes in certain disease states.[8–12]

Our long-term goal is to establish the relationship between retinal structure and cone- and rod-mediated visual function at all stages along a subretinal drusenoid deposit (SDD)-driven pathway to advanced age-related macular degeneration (AMD) distinct from that driven by drusen.[13–18] First seen in 1990,[19] SDD (also called reticular pseudodrusen or pseudodrusen) was established as extra cellular lesions located between the retinal pigment epithelium (RPE) and photoreceptors with optical coherence tomography (OCT) and

histology in 2010[20] and later shown to portend poor vision.[16,21] Histology shows deflection, shortening, and disappearance of both cones and rods around SDD in AMD eyes.[14] Our current approach is longitudinal imaging the cone photoreceptor structure in parafovea and perifovea using confocal AOSLO in subjects with and without intermediate to advanced AMD.[18,22,23]

Imaging elderly patients with AMD is challenged by age-related degradation of ocular optics, in several aspects. First, in most aging eyes, pupil size decreases[24] and ocular wavefront aberration increases.[25–28] Second, many older patients have cataract,[29] which significantly impairs wavefront detection and correction by adaptive optics (AO).[3] Third, of the elderly who have had cataract surgery and implanted intraocular lenses (IOL), the clear optical window is reduced (<7 mm).[30] More than 25% will develop posterior capsular opacification (PCO) or fibrosis on the IOL due to proliferation and transformation of remaining lens epithelial cells.[31,32] While capsulotomy via laser can open the opacified posterior capsule, the clear aperture for imaging often has an irregular shape.[33] This may not only reduce the useful optical pupil size but also complicate light scattering and impede AO operation. Furthermore, age- and pathology-related scattering in the lens, vitreous and retina, can markedly reduce the photons available for imaging. Consequently, AOSLO has been mostly used in research applications involving young and middle-aged adults who generally have good ocular media clearity.[3] To translate AOSLO for patient care and clinical trials for AMD and other conditions affecting older adults, the impact of lens opacity on AOSLO imaging of aged eyes deserves to be critically assessed. This may be achieved by characterizing lens opacity, including pseudophakic lens capsule opacification, and correlating these findings with AOSLO image quality.

As a relatively new imaging technique, AOSLO does not have any established grading systems for assessing its image quality. Resolution, signal to noise ratio, contrast, and sharpness may be affected both by imaging system performance and by retinal pathology. Because AOSLO's major technical advantage is high image resolution that reveals individual photoreceptors[2,4] and confocal AOSLO imaging of photoreceptors relies on the waveguiding property of photoreceptors,[34] we proposed an heuristic grading method using cone photoreceptor visibility as a main criterion for assessing AOSLO image quality in this study. While rods are affected early in AMD and will be more useful for studying pathophysiology,[35] they are at the resolution limit of AOSLO[8] and are thus difficult to image in aged eyes. On the other hand, cones are surrounded and supported by rods,[35] and both are affected in AMD.[13,14,35] Thus, cone reflectivity may help infer rod health status. We enrolled 80 elderly participants with and without AMD. To assess AMD presence and severity, we acquired color fundus photographs following the Age-Related Eye Disease Study (AREDS) imaging protocol.[36] We assessed the subjects' lens opacities using stereoscopic digital fundus reflex photographs following the AREDS2 lens opacity grading system.[37] We found that the AOSLO could acquire useful cone photoreceptor images in the majority of older eyes.

Methods

Compliance

This study involving human participants followed the tenets of the Declaration of Helsinki and the Health Insurance Portability and Accountability Act of 1996. It was approved by the Institutional Review Board at the University of Alabama at Birmingham and the University of California–Los Angeles. Written informed consent was obtained from participants after the nature and possible consequences of the study were explained.

Subject Recruitment

Study patients with AMD and age-similar subjects in normal chorioretinal health were recruited from the clinical research registry of the Department of Ophthalmology and Visual Sciences of the University of Alabama at Birmingham and through its Retina Service. A clinical research coordinator identified from the medical record patients who had been previously diagnosed with AMD with best-corrected visual acuity (BCVA) of 20/400 or better. A senior researcher (CO) reviewed the selected clinical charts. Exclusion criteria included diabetes, glaucoma, history of retinal vascular occlusions and hereditary retinal dystrophy. The inclusion criteria for normal subjects were age >50 years old, no history of ocular and systemic disease, and BCVA of 20/25 or better. Refractive errors determined from the medical record were within ±6 D spherical and ±3 D cylinder for all participants.

AMD Presence and Severity

Color digital 30° fundus photographs were taken (FF450 Plus fundus camera; Carl Zeiss Meditec, Dublin, CA, USA) after pupil dilation. Photographs were graded by a masked, experienced grader (M.E.C.)

using the Age-Related Eye Disease Study (AREDS) 9-step severity scale for AMD.[36] To include patients with advanced AMD, we extended this grading system with two additional steps: step 10 for central geographic atrophy and step-11 for neovascularization. Thus, disease severity ranged from early to advanced (AREDS steps 2–11). Participants in normal macular health met the criteria for AREDS grade 1 in both eyes.

AOSLO

The instrument has been described[38] and is summarized here. The AOSLO works in the confocal imaging mode using an infrared low coherence light source (Superluminescent diode HP 840; Superlum Ltd, Moscow, Russia; $\lambda = 840$ nm, $\Delta\lambda = 50$ nm) that minimizes light interference artifact. The AO system consists of high-speed components (custom designed Shack-Hartmann wavefront sensor and deformable mirror) that enable a closed-loop frequency up to 100 Hz.[11] The deformable mirror has 97 actuators with stroke up to 30 µm to compensate for the increased wave aberration in aged eyes. AOSLO retinal image registration was aided by high-speed sub-pixel image registration software based on a parallel graphic processing unit technique.[38,39]

The AOSLO was implemented with control strategies for correcting wave aberration in pupils with irregular shapes and non-uniform illumination. The zonal correction algorithm minimized local wavefront gradients or slopes,[40,41] and the modal correction method minimizes the Zernike modes of the wavefront.[1,42] The Zernike mode-based algorithm was used for cases with missing wavefront sampling points due to locally thick cataract or irregularly shaped pupils. Additionally, to mitigate the effect of nonuniform light spots due to lens opacity on the Shack-Hartmann wavefront sensor, we designed a two-step exposure method. This entailed taking two snapshots of the wavefront with a longer then shorter exposure time. Saturated light spots taken in the long exposure were replaced by spots imaged with the short exposure.

Imaging Protocol

After the consenting process, the participant underwent BCVA measurement by the Electronic Visual Acuity (EVA) protocol.[43] Then the subject's pupil was dilated with one to two drops of 1.0% tropicamide and 2.5% phenylephrine. After 15 to 20 minutes, AOSLO was performed; the subject's head was aligned and stabilized using a head-mount with a chin-rest. The subject was instructed to fixate on a target consisting of a moving green light dot on a calibrated grid, shown on the back of grid paper, through a dichroic mirror. At the beginning of every image acquisition session, we ensured subject fixation on the target and focused the imaging light on cone inner segments. During imaging, the dot was moved along the grid to direct the subject's view. At each grid point, the light dot stopped for three to five seconds, during which time 45 to 75 frames were acquired. Video was recorded continuously across an area of 15° × 15° to 20° × 20°. An AOSLO session often lasted 30 to 45 minutes for imaging both eyes. For eyes with successfully acquired images, montages were created.

After AOSLO imaging, three-field digital color fundus photographs[36] and stereoscopic fundus reflex photographs of both eyes were taken using the AREDS protocol. The subject's gaze was directed by a fixation target to avoid the impact of the optic nerve head on fundus reflex. Image focus was maintained on the pupillary margin. The photographer (M.E.C.) was certified by the AREDS Reading Center at the University of Wisconsin.

Grading of the Lens Opacity

We assessed the lens opacity of the subjects following the method reported by Domalpally and coworkers.[37] The lens of the study eye was classified as phakic (original) or pseudophakic (with IOL). Lens status was ascertained using fundus reflex images. In general, a single central light reflex indicates a phakic lens. More than one reflex indicates a pseudophakic IOL. Furthermore, eyes with IOLs may have a lens capsule visible on the back or edge of the lens.

Currently available lens opacity grading systems are designed for evaluating cataract in eyes with original lenses only.[37,44–46] There is no published systematic method for estimating opacity in eyes with pseudophakic IOLs. To assess lens opacity in subjects with original lenses and in those with IOLs, we adopted the AREDS Clinical Lens Grading Protocol. This system classifies opacity into three types: nuclear opalescence (by nuclear cataract [NC]), cortical opacity (by cortical cataract: CC), and posterior subcapsular (PSC) opacity. The severity of each type is divided into six grades: 0.0, no cataract; 1.0, cataract standard 1; 2.0, cataract standard 2; 3.0, cataract standard 3; 4.0, completely opacified; 8, cannot evaluate).[46] For phakic subjects, we assessed PSC and CC using the fundus reflex photograph (Fig. 1). As opacity caused by NC could not be assessed from the fundus reflex image, we used the notation of lens clarity in the patient's most recent medical record. For pseudophakic subjects, we evaluated PCO by position and coverage (Fig. 1), similar to the assessment of PSC and CC. The

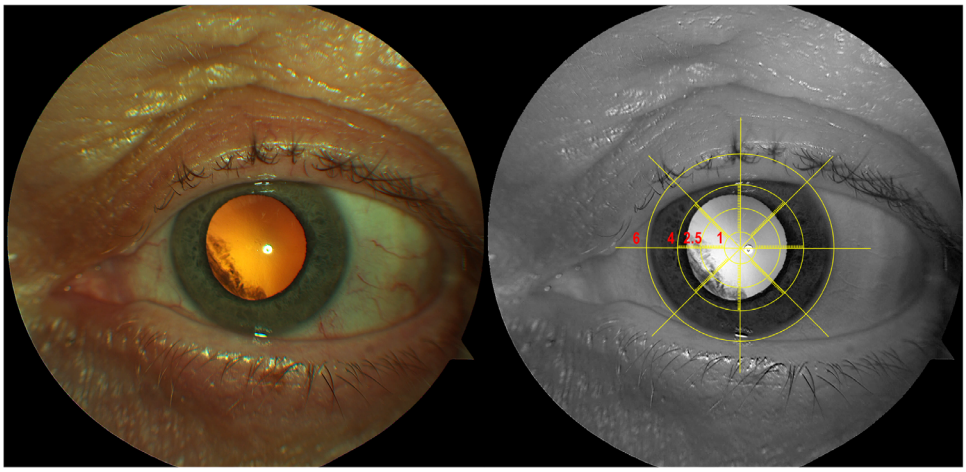

Figure 1. Color fundus reflex image (left) and enhanced red channel image with the modified AREDS grid (right). Color fundus reflex imager shows cortical cataract. To assess the extent of cataract, the red channel image is overlaid with a modified AREDS lens grid.[37,45]

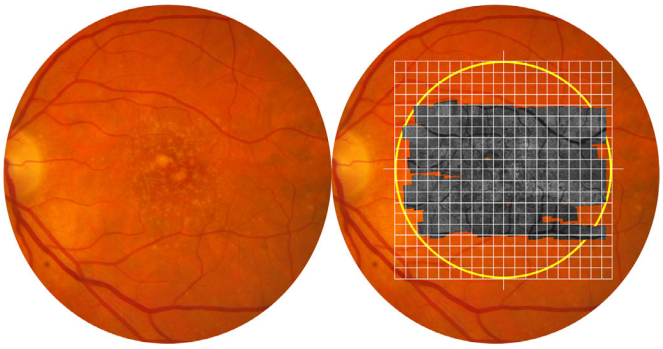

Figure 2. Grading of the image quality of AOSLO. Shown is the fundus of a patient with AREDS grade 6. Yellow circle on right panel delimits the central 20° (i.e., the macula). The gray image is an AOSLO montage overlaid on the color fundus photograph. Grid squares are 1° × 1°. Cone photoreceptor visibility was examined in each grid square and classified as 'resolved' or 'unresolved.'

red channel of the fundus reflex image was extracted using image processing software (Adobe Photoshop CC, Adobe Systems Inc, San Jose, CA). Brightness and contrast were optimized to display lens clarity. Lens opacity was assessed within the central 5-mm-diameter zone of a modified AREDS lens grid (Fig. 1). Opacity was expressed as percentage of 16 subfields and the central circle of the lens grading grid.[37] The total opacity degree was in 10 grades (0–9), with 0 representing perfectly clear lens and larger number indicting deteriorated clarity.

Grading of the AOSLO Image Quality

To evaluate the AOSLO image quality, we put a sampling grid with a 1° interval over the macula (Fig. 2). We classified the visibility of cones in each grid square as "resolved" or "unresolved." The (patch of) image was deemed 'cone-resolved' if cones were clearly seen in a characteristic mosaic pattern anywhere within this grid (Figs. 3A, 3C, and 3D), whereas the image would be considered as "cone-unresolved" if cones were not clearly revealed (Fig. 3B). Figure 3 presents examples illustrating cone visibility quality in AOSLO images of eyes at different stages of AMD. In eyes at AREDS grade 1, an image with well-resolved cones shows a contiguous cell mosaic across the entire 1° × 1° grid (Fig. 3A). In eyes with dense lenticular opacity, AOSLO could produce blurry retinal images with large vascular structures only (Fig. 3B). This image patch is "cone-unresolved." In eyes with AMD, cone reflectivity may be affected by AMD's extracellular lesions at early and intermediate stages and by atrophic or neovascular processes at advanced stages. Cone appearance is determined by cell visualization near or outside the affected area. If (clusters of) cones are imaged with the characteristic mosaic pattern (red arrowheads, Figs. 3C and 3D), the image is considered as "cone-resolved."

Based on the percentage of cone-resolved images across the whole montage, we classified the entire AOSLO montage as one of 3 grades: good, adequate, and inadequate. For good image quality, in a large montage $\geq$ 15° × 15° (but not necessarily square), cone photoreceptors were resolved on $\geq$ 90% of the entire montage (Supplementary Figs. S1 and S2). For adequate image quality, a large montage $\geq$ 15° × 15° could be made, and cones were resolved on $\geq$ 75% but $<$ 90% of total sampling points (Supplementary Fig. S3). For Inadequate image quality, images could be acquired but cones were resolved on $<$75% of retinal montage (Supplementary Fig. S4).

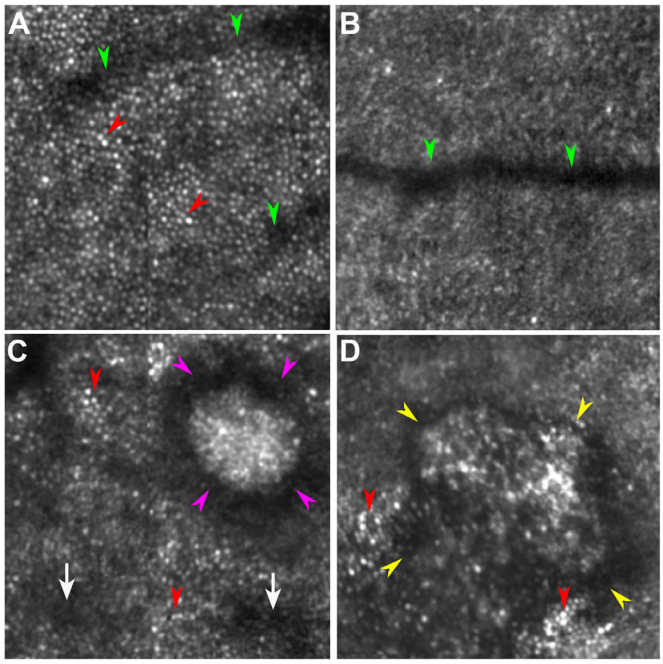

Figure 3. Cone visualization in AOSLO images. A. An image showing well-resolved cones was taken in the eye of a normal subject (AREDS AMD grade 1). Hyporeflective bands are shadows cast by a retinal capillary (green arrowheads). Cones are manifest as reflective dots packing in a contiguous mosaic pattern (red arrowheads). B. An image with unresolved cones taken in the eye of a normal subject (AREDS grade 1). While a retinal vessel is imaged (green arrowheads), a cone mosaic is not visible. C. An image showing resolved cones taken in the eye of a patient with AREDS grade 8. Although cones lose reflectivity due to perturbation by subretinal drusenoid deposits (stage 3, magenta arrowheads; stage 1, white arrows), the characteristic cone mosaic is still visible outside the area directly affected by the lesion (red arrowheads). D. An image showing resolved cones taken in the eye of a patient with AREDS grade 7. Characteristic cone mosaic (red arrowheads) is visible outside an atrophic area (yellow arrowheads). All the images are 1° × 1° and were acquired at approximately 2° superior to the foveal center. Corresponding pupil images and lens clarity of these eyes are shown in Figure 5.

To verify the reliability of AOSLO image quality grading, two authors assessed the images independently, and agreement was determined by Cohen's κ statistic.

Results

A total of 80 subjects (41 males and 39 females, aged 72.5 ± 11.5 years) were enrolled (Table), and 159 eyes were examined. One eye was excluded due to cornea damage. Sixteen subjects (age 68.3 ± 8.7 years old) were in normal chorioretinal health, i.e., both eyes were of AREDS grade 1. Sixty-four subjects (age: 74.7 ± 7.0 years old, $P = 0.001$) with AMD in at least one eye were graded at AREDS 2-11. Dilated pupil diameters of normal subjects and patients with AMD were 6.1 ± 1.0 mm and 6.2 ± 0.9 mm ($P = 0.35$), respectively. However, pupil shape in most eyes was irregular. The average diameter of pupils undergoing AOSLO imaging was 5.6 mm. The BCVA (converted to logarithm of the minimum angle of resolution) of normal subjects and patients with AMD was 0.10 ± 0.11 and 0.23 ± 0.29 ($P = 0.006$), respectively. The opacity of normal subjects and patients with AMD was 2.0 ± 1.7 and 3.2 ± 2.0 mm ($P = 0.001$), respectively.

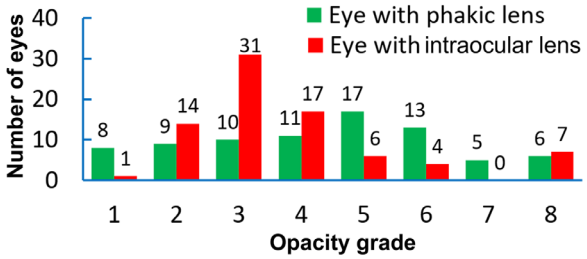

Figure 4. Frequency of opacity grades stratified by lens in the study eyes. Total eyes: 159. Eyes with phakic lenses: 79; eyes with pseudophakic intraocular lenses: 80.

AOSLO can image cone photoreceptors in patients with various stages of AMD through cataracts or IOLs, with individual opacities caused by NSC, PSC, CC, or PCO, up to grade 2.5 (Figs. 4–6). Of 159 eyes, the AOSLO produced Good images in 91 eyes (57%), Adequate images in 8 eyes (5%), and Inadequate images in 27 eyes (17%). Cones could be imaged with Good quality when overall lens clarity was better than grade 6 (Fig. 6A) in subjects of all stages of AMD (Fig. 6B). Good and adequate images could be acquired from 25% to 100% of eyes with AMD at different stages (Fig. 6C). AOSLO produced good and adequate images in 61% of normal eyes and in 63% of AMD eyes, respectively.

Forty-two (n = 42) eyes were imaged with the Zernike modal control (26 good images, 4 adequate, 12 inadequate). Seven (n = 7) eyes were imaged with the two-step wavefront detection (four good images, zero adequate, three inadequate), and 77 eyes were imaged with the zonal control algorithm.

AOSLO could not obtain images in 33 eyes (21%) for these reasons. First was a high degree of overall opacity > 6.5 (15 eyes, 9 subjects). In these cases, the wavefront sensor could not provide reliable detection of wave aberration for AO correction. No high-resolution retinal images could be acquired. Second was a small pupil < 5 mm (11 eyes, seven subjects). Under this condition, the useful pupil was smaller than that necessary for taking advantage of

Table. Characteristics of the Study Eyes

AREDS* Grades	Number of Eyes	Percentage of Sample	Logmar (Mean ± SD)
1†	31	19%	0.10 ± 0.11
1‡	11	7%	0.17 ± 0.16
2	16	10%	0.14 ± 0.14
3	3	2%	0.07 ± 0.05
4	13	8%	0.11 ± 0.13
5	9	6%	0.20 ± 0.19
6	32	20%	0.10 ± 0.10
7	10	6%	0.24 ± 0.19
8	7	4%	0.22 ± 0.17
9	4	3%	0.23 ± 0.08
10	14	9%	0.55 ± 0.47
11	9	6%	0.58 ± 0.44

LogMAR, Logarithm of the Minimum Angle of Resolution.
*Age-Related Eye Disease Study.
†Both eyes were AREDS grade 1.
‡One eye was AREDS grade 1.

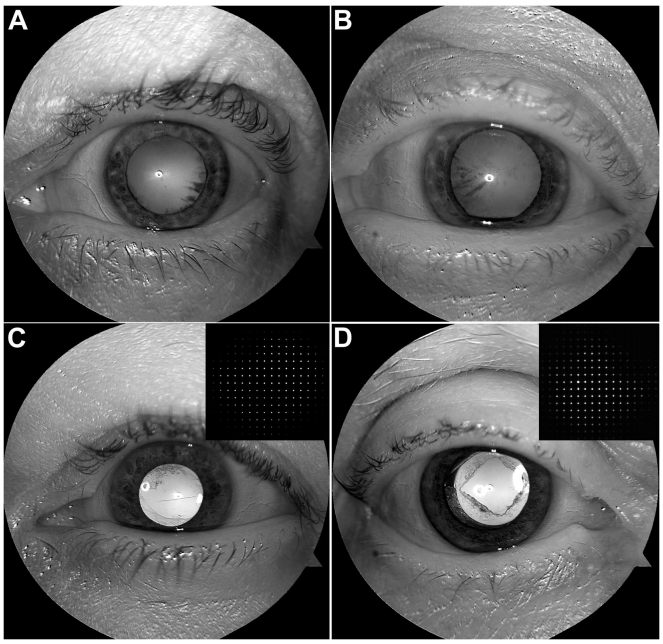

Figure 5. Enhanced red channel of the color fundus reflex images showing pupil shape and lens clarity. Insets show the sampling points on the Shack-Hartmann wavefront sensor through the irregular pupil. Corresponding retinal images taken from these eyes are shown in Figure 3. A. Overall opacity grade is 3.5, including nuclear opacity (NUC) 2.5 and cortical cataract (CC) 1. B. Overall opacity grade is 7.5, including NUC 2.0 and CC 3, and PSC 2.5. C. IOL with cortical posterior capsular opacification (PCO grade 1). D. IOL with cortical PCO grade 2.5.

AO wavefront compensation. Third was problems specific to individual subjects, such as sleep, drooping eyelid, inability to keep eye open, and failure to attend the AOSLO imaging session (seven eyes, four subjects). These subjects were neither further imaged by AOSLO nor offered another imaging session. There was a high agreement between the two raters' assessment of the AOSLO image grade, $\kappa = 0.92$ (95% CI, 0.88 to 0.96), $P < 0.001$.

Discussion

In this study, we evaluated AOSLO performance in imaging cone photoreceptors in elderly human subjects across a range of ocular opacities due to cataracts in phakic lenses and posterior capsular opacification (including eyes that had been treated with laser capsulotomy) of IOLs. Our data indicate that AOSLO can produce images good or adequate for assessing cones in more than 60% of study eyes. Notably these eyes had not undergone a comprehensive prescreening of ocular optics.

AO-assisted en face imaging, including AO flood illumination fundus camera and AOSLO, is a powerful tool for research on AMD that may also play an important role in diagnosis and treatment of AMD in large clinical settings.[47] The major benefit of AO imaging is high spatial resolution that enables AO correction for aberrations caused by the ocular optical defects.[2–4,48] Complex light scattering, light reduction, and pupil irregularity caused by cataract, posterior capsular opacification of the IOL, and capsulotomy cannot be compensated by the AO. Confocal imaging rejects out-of-focus scattering, thereby

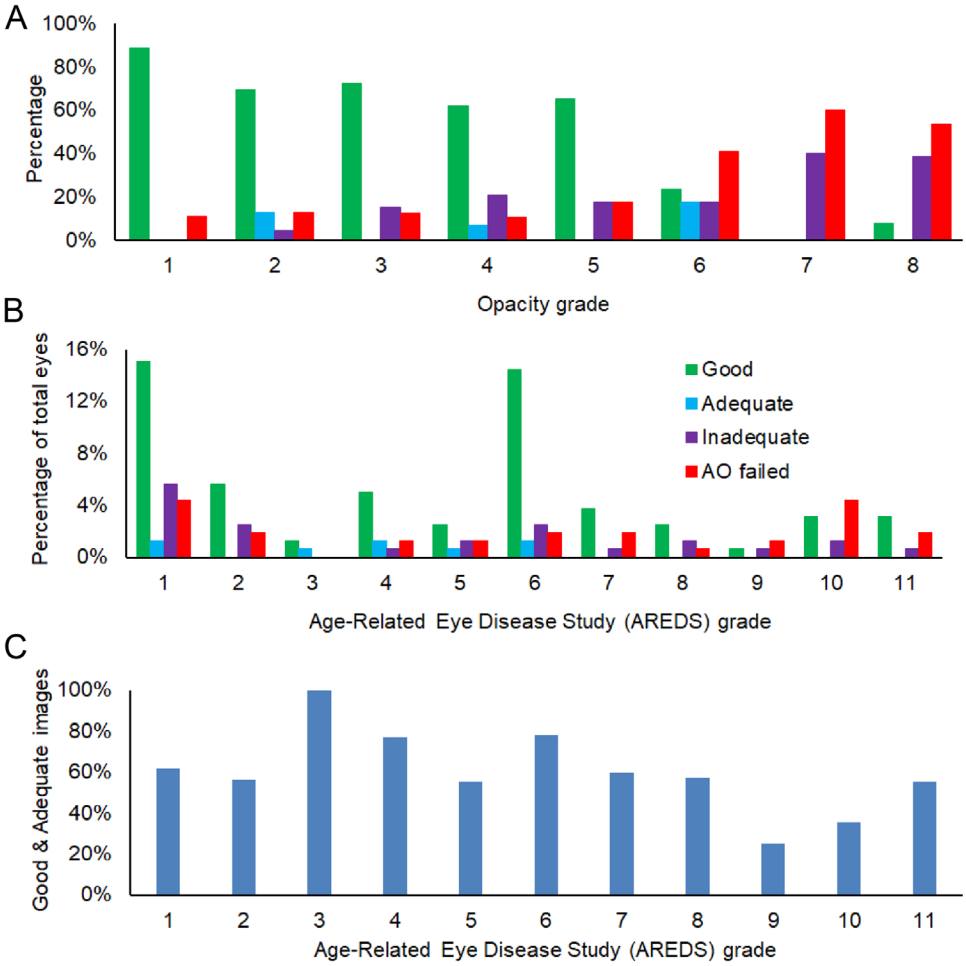

Figure 6. AOSLO image quality in study eyes. A. Distribution of AOSLO images considered good, adequate, inadequate, and AOSLO failed to acquire images, with different lens opacities. B. Distribution of AOSLO images considered good, adequate, inadequate, and AOSLO failed to acquire images, with different AREDS grades. C. Good and adequate images acquired in eyes with different AREDS grades.

enhancing image contrast of cone structure and optical properties.[2–4] In a previous study of AMD using AOSLO, subjects were carefully selected by an experienced clinical expert to have a pupil ≥7 mm and to lack dense cataract or other media opacities.[49] In this study, a relatively large number of older subjects were enrolled. The main initial assessment of optical quality was visual acuity on medical records (normal 20/25, AMD 20/400). Subjects underwent no further examination of optical media before AOSLO imaging. Although the percentage of eyes in which AOSLO did not acquire useful images may seem large (33 eyes in 25 consented subjects, 21% of the sample), 18 eyes were not imaged due to nontechnical reasons that might occur in any study of older adults. Since AOSLO's image resolution is fundamentally determined by the pupil size, a large pupil is desirable, which is typically achieved by pharmacologic dilation. If the pupil is small, e.g., <5 mm (11 eyes, seven subjects), the benefit of the AO is diminished. Thus we strive to image eyes with a pupil large enough to take advantage of AO, and we used mydriatic drugs (1.0% tropicamide and 2.5% phenylephrine) most commonly used in ophthalmic and optometric practices.

Although good image quality was best achieved in eyes with low lens opacity (Fig. 6A), we also found that good image quality could be achieved in eyes with AMD at any stage (Figs. 6B and 6C). In a study involving a group of 40 asymptomatic subjects with known genetic relative risk for developing AMD, Land and coworkers[50] reported that cones were discernable in 55% of the study eyes using confocal AOSLO. Our study included clinically diagnosed AMD patients across all stages and older normal subjects (mean age 72.5 years vs. 61.4 years in the Land study). Thus we demonstrate here that AOSLO can image cones in older eyes with a satisfactory quality with an even larger success rate. We believe that in future applications, the AOSLO

can achieve higher rates of good image quality, with close attention to the pupil state and ocular media in patients who lack characteristics that preclude AOSLO imaging.

It is worth mentioning our strategies to facilitate imaging through aged eyes. First, we devised wavefront reconstruction methods specific to technical challenges imposed by cataract and posterior capsule opacification. Our AOSLO operates with a classic AO, i.e., a wavefront sensor to measure wave aberration and a deformable mirror to compensate the aberration dynamically through a closed-loop feedback control scheme. This regime requires accurate measurement of wave aberration over the entire pupil aperture. Missing light spots on the sub-apertures of the Shack-Hartmann wavefront sensor makes the wavefront reconstruction matrix[41,51] ineffective. This problem has been a leading cause of failure of AO in our zonal correction algorithm. Under this situation, wavefront reconstruction using Zernike modes as we did is an effective solution, since it can reconstruct the wavefront even when some sampling spots were missing.

Second, while fixation stability is not hampered in older adults with good acuity (i.e., normal, early AMD, and intermediate AMD),[52,53] it is problematic in advanced AMD impacting central vision, making it difficult to maintain image topography inside the eye. Spatial properties (e.g., density, spacing) of the cone mosaic is highly dependent on distance from the fovea, which is therefore captured in addition to specific regions of interest in large montages.[54] A large montage in turn requires continuous recording of retinal images while the eye is following a moving fixation target. To compensate for intrinsically dynamic variations of the ocular wave aberration and variation introduced by eye movements to follow the target,[40,55–58] it is critical for the AO to operate with high speed. Our AOSLO is equipped with a custom Shack-Hartmann wavefront sensor that ensures a high frequency closed-loop up to 100 Hz and robust correction for wave aberration.[11,59] Despite reduced back-scattered imaging light in aged eyes that prevents operation at 100 Hz in all eyes, we could maintain a loop frequency of $\geq$50 Hz in most eyes, to ensure that wave aberration was corrected during continuous image acquisition.

Since we used the visibility of cones as the main criterion for image quality, it is necessary to estimate the actual image resolution achieved in aging eyes. In this study, while the pupil could be dilated to 6.2 mm diameter on average, pupils were irregularly shaped in most eyes. Consequently, the AO correction was conducted on an average pupil diameter of 5.6 mm, which theoretically yields an image resolution $\sim$3.0 µm with an imaging light wavelength of 840 nm. Therefore, it is conceivable that in most eyes cone photoreceptors can be resolved at 0.5° from the foveal center and beyond. In contrast, rods cannot be reliably resolved in the macula. Given the significance of rods in AMD pathophysiology,[35,60] short wavelength light can be considered in studies targeting rod structure.[8,12] In addition, AOSLO using off-axis imaging technique[7] or split-detection[61] are useful for imaging cones in AMD, especially when cone misalignment or shortening due to by pathology impacts waveguiding.

Study strengths include quantification of AOSLO imaging performance in a large number of aged eyes, without strict prescreening for ocular media characteristics. Of the study eyes, natural lenses and IOLs each appeared in half of the total eyes, which reflects the IOL characteristics of older adults in our geographic region.[62] Our grading system and estimation of AO image quality may assist prediction of AOSLO imaging outcome and help investigators decide the subject number and budget for clinical trials. Limitations addressable in future work include subjective image quality based upon cone visualization only, which is a necessary first step before determining repeatability of cone assessments. Another limitation is that lens opacity grading was based upon fundus reflex only and does not include nuclear cataract. A slit lamp examination can be used to assess cataract presence and severity using the Lens Opacities Classification System III.[63] Simple and inexpensive diagnostic methods of lens status are thus desirable. In conclusion, despite challenges from optics of the aging eye, AOSLO has promise for large clinical trials for older patients with retinal diseases and for observational studies relating cellular morphology to visual function.

Acknowledgments

The authors thank C. Douglas Witherspoon, Richard Feist, Jr., and Christopher A. Girkin for helping with patient recruitment and clinical support and Karen Searcey for help with research administration. The authors also acknowledge the technical assistance by Jinyu Wang, Angelia Johnson, Yongxin Yu, Alexander Meadway, Ernesto Blanco, Tianjiao Zhang, Pooja Godara, and Boyu Gu.

Supported by NIH R01EY024378, R21EY027948, R01EY029595, R01AG04212, P30EY003039, and institutional support from Doheny Eye Institute, Research to Prevent Blindness, EyeSight Foundation of Alabama, the Carl G. and Pauline Buck Trust, the Alfreda J. Schueler Trust, and the Dorsett Davis

Discovery Fund. The funding organizations had no role in the design or conduct of this research.

Disclosure: **Y. Zhang,** None; **X. Wang,** None; **M.E. Clark,** None; **C.A. Curcio,** Heidelberg Engineering, Inc. (R), Genentech, Inc. (R); **C. Owsley,** None

* Christine A. Curcio and Cynthia Owsley contributed equally to this article.

References

1. Roorda A, Romero-Borja F, Donnelly Iii W, Queener H, Hebert T, Campbell M. Adaptive optics scanning laser ophthalmoscopy. *Opt Express*. 2002;10:405–412.
2. Roorda A, Duncan JL. Adaptive optics ophthalmoscopy. *Annu Rev Vis Sci*. 2015;1:19–50. [PubMed].
3. Marcos S, Werner JS, Burns SA, et al. Vision science and adaptive optics, the state of the field. *Vision Res*. 2017;132:3–33. [PubMed].
4. Burns SA, Elsner AE, Sapoznik KA, Warner RL, Gast TJ. Adaptive optics imaging of the human retina. *Prog Retin Eye Res*. 2019;68:1–30. [PubMed].
5. Chui TYP, Vannasdale DA, Burns SA. The use of forward scatter to improve retinal vascular imaging with an adaptive optics scanning laser ophthalmoscope. *Biomed Opt Express*. 2012;3:2537–2549.
6. Scoles D, Sulai YN, Langlo CS, et al. In vivo imaging of human cone photoreceptor inner segments. *Invest Ophthalmol Vis Sci*. 2014;55:4244–4251. [PubMed].
7. Rossi EA, Granger CE, Sharma R, et al. Imaging individual neurons in the retinal ganglion cell layer of the living eye. *Proc Natl Acad Sci*. 2017;114:586–591.
8. Dubra A, Sulai Y, Norris JL, et al. Noninvasive imaging of the human rod photoreceptor mosaic using a confocal adaptive optics scanning ophthalmoscope. *Biomed Opt Express*. 2011;2:1864–1876. [PubMed].
9. Cooper RF, Dubis AM, Pavaskar A, Rha J, Dubra A, Carroll J. Spatial and temporal variation of rod photoreceptor reflectance in the human retina. *Biomed Opt Express*. 2011;2:2577–2589. [PubMed].
10. Merino D, Duncan JL, Tiruveedhula P, Roorda A. Observation of cone and rod photoreceptors in normal subjects and patients using a new generation adaptive optics scanning laser ophthalmoscope. *Biomed Opt Express*. 2011;2:2189–2201.
11. Yu Y, Zhang T, Meadway A, Wang X, Zhang Y. High-speed adaptive optics for imaging of the living human eye. *Opt Express*. 2015;23:23035–23052. [PubMed].
12. Wells-Gray EM, Choi SS, Bries A, Doble N. Variation in rod and cone density from the fovea to the mid-periphery in healthy human retinas using adaptive optics scanning laser ophthalmoscopy. *Eye (Lond)*. 2016;30:1135–1143. [PubMed].
13. Chen L, Messinger JD, Zhang Y, Spaide RF, Freund KB, Curcio CA. Subretinal drusenoid deposit in age-related macular degeneration: Histologic insights into initiation, progression to atrophy, and imaging. *Retina*. 2020;40:618–631. [PubMed].
14. Curcio CA, Messinger JD, Sloan KR, McGwin G, Medeiros NE, Spaide RF. Subretinal drusenoid deposits in non-neovascular age-related macular degeneration: Morphology, prevalence, topography, and biogenesis model. *Retina*. 2013;33:265–276. [PubMed].
15. Spaide RF. Outer retinal atrophy after regression of subretinal drusenoid deposits as a newly recognized form of late age-related macular degeneration. *Retina*. 2013;33:1800–1808.
16. Spaide RF, Ooto S, Curcio CA. Subretinal drusenoid deposits aka pseudodrusen. *Surv Ophthalmol*. 2018;63:782–815.
17. Xu L, Blonska AM, Pumariega NM, et al. Reticular macular disease is associated with multilobular geographic atrophy in age-related macular degeneration. *Retina*. 2013;33:1850–1862. [PubMed].
18. Zhang Y, Wang X, Sadda SR, et al. Lifecycles of individual subretinal drusenoid deposits and evolution of outer retinal atrophy in age-related macular degeneration. *Ophthalmology Retina*. 2020;4:274–283. [PubMed].
19. Mimoun G, Soubrane G, Coscas G. [macular drusen]. *J Fr Ophtalmol*. 1990;13:511–530.
20. Zweifel SA, Spaide RF, Curcio CA, Malek G, Imamura Y. Reticular pseudodrusen are subretinal drusenoid deposits. *Ophthalmology*. 2010;117:303–312.e301.
21. Flamendorf J, Agron E, Wong WT, et al. Impairments in dark adaptation are associated with age-related macular degeneration severity and reticular pseudodrusen. *Ophthalmology*. 2015;122:2053–2062. [PubMed].
22. Zhang Y, Wang X, Rivero EB, et al. Photoreceptor perturbation around subretinal drusenoid deposits as revealed by adaptive optics scanning laser ophthalmoscopy. *Am J Ophthalmol*. 2014;158:584–596.e581. [PubMed].

23. Zhang Y, Wang X, Godara P, et al. Dynamism of dot subretinal drusenoid deposits in age-related macular degeneration demonstrated with adaptive optics imaging. *Retina*. 2018;38:29–38. [PubMed] PMC5552451.
24. Birren JE, Casperson RC, Botwinick J. Age changes in pupil size. *J Gerontol*. 1950;5:216–221.
25. Amano S, Amano Y, Yamagami S, et al. Age-related changes in corneal and ocular higher-order wavefront aberrations. *Am J Ophthalmol*. 2004;137:988–992.
26. Fujikado T, Kuroda T, Ninomiya S, et al. Age-related changes in ocular and corneal aberrations. *Am J Ophthalmol*. 2004;138:143–146.
27. Rocha KM, Nose W, Bottos K, Bottos J, Morimoto L, Soriano E. Higher-order aberrations of age-related cataract. *J Cataract Refract Surg*. 2007;33:1442–1446.
28. Sachdev N, Ormonde SE, Sherwin T, McGhee CN. Higher-order aberrations of lenticular opacities. *J Cataract Refract Surg*. 2004;30:1642–1648.
29. Foster A. Vision 2020: The cataract challenge. *Community Eye Health*. 2000;13:17–19.
30. Erie JC, Hardwig PW, Hodge DO. Effect of intraocular lens design on neodymium:Yag laser capsttlotomy rates. *Journal of Cataract & Refractive Surgery*. 1998;24:1239–1242.
31. Hollick EJ, Spalton DJ, Ursell PG, et al. The effect of polymethylmethacrylate, silicone, and polyacrylic intraocular lenses on posterior capsular opacification 3 years after cataract surgery. *Ophthalmology*. 1999;106:49–54; discussion 54-45.
32. Schaumberg DA, Dana MR, Christen WG, Glynn RJ. A systematic overview of the incidence of posterior capsule opacification. *Ophthalmology*. 1998;105:1213–1221.
33. Khambhiphant B, Liumsirijarern C, Saehout P. The effect of nd:Yag laser treatment of posterior capsule opacification on anterior chamber depth and refraction in pseudophakic eyes. *Clin Ophthalmol*. 2015;9:557–561. [PubMed].
34. Roorda A, Williams DR. Optical fiber properties of individual human cones. *Journal of Vision*. 2002;2:4–4.
35. Curcio CA, Owsley C, Jackson GR. Spare the rods, save the cones in aging and age-related maculopathy. *Invest Ophthalmol Vis Sci*. 2000;41:2015–2018.
36. Davis MD, Gangnon RE, Lee LY, et al. The age-related eye disease study severity scale for age-related macular degeneration: Areds report no. 17. *Arch Ophthalmol*. 2005;123:1484–1498. [PubMed].
37. Domalpally A, Danis RP, Chew EY, et al. Evaluation of optimized digital fundus reflex photographs for lens opacities in the age-related eye disease study 2: Areds2 report 7. *Invest Ophthalmol Vis Sci*. 2013;54:5989–5994. [PubMed].
38. Meadway A, Girkin CA, Zhang Y. A dual-modal retinal imaging system with adaptive optics. *Opt Express*. 2013;21:29792–29807. [PubMed].
39. Vogel CR, Arathorn DW, Roorda A, Parker A. Retinal motion estimation in adaptive optics scanning laser ophthalmoscopy. *Opt Express*. 2006;14:487–497.
40. Hofer H, Chen L, Yoon GY, Singer B, Yamauchi Y, Williams DR. Improvement in retinal image quality with dynamic correction of the eye's aberrations. *Opt Express*. 2001;8:631–643.
41. Li KY, Mishra S, Tiruveedhula P, Roorda A. Comparison of control algorithms for a mems-based adaptive optics scanning laser ophthalmoscope. *Proc Am Control Conf*. 2009;2009:3848–3853. [PubMed].
42. Zhang Y, Poonja S, Roorda A. Mems-based adaptive optics scanning laser ophthalmoscopy. *Opt Lett*. 2006;31:1268–1270.
43. Beck RW, Moke PS, Turpin AH, et al. A computerized method of visual acuity testing: Adaptation of the early treatment of diabetic retinopathy study testing protocol. *Am J Ophthalmol*. 2003;135:194–205.
44. Klein BE, Klein R, Linton KL, Magli YL, Neider MW. Assessment of cataracts from photographs in the beaver dam eye study. *Ophthalmology*. 1990;97:1428–1433.
45. The Age-Related Eye Disease Study Research Group. The age-related eye disease study (AREDS) system for classifying cataracts from photographs: AREDS report no. 4**members of the age-related eye disease study research group are listed at the end of the article. *Am J Ophthalmol*. 2001;131:167–175.
46. Chew EY, Kim J, Sperduto RD, et al. Evaluation of the age-related eye disease study clinical lens grading system areds report no. 31. *Ophthalmology*. 2010;117:2112–2119.e2113. [PubMed].
47. Paques M, Meimon S, Rossant F, et al. Adaptive optics ophthalmoscopy: Application to age-related macular degeneration and vascular diseases. *Prog Retin Eye Res*. 2018;66:1–16.
48. Liang J, Williams DR, Miller DT. Supernormal vision and high-resolution retinal imaging through adaptive optics. *J Opt Soc Am A Opt Image Sci Vis*. 1997;14:2884–2892.
49. Zayit-Soudry S, Duncan JL, Syed R, Menghini M, Roorda AJ. Cone structure imaged with adaptive optics scanning laser ophthalmoscopy in eyes with nonneovascular age-related macular

degeneration. *Invest Ophthalmol Vis Sci*. 2013;54:7498–7509. [PubMed].
50. Land ME, Cooper RF, Young J, et al. Cone structure in subjects with known genetic relative risk for amd. *Optom Vis Sci*. 2014;91:939–949. [PubMed].
51. Hofer H, Chen L, Yoon GY, Singer B, Yamauchi Y, Williams DR. Improvement in retinal image quality with dynamic correction of the eye's aberrations. *Opt Express*. 2001;8:631–643.
52. Kosnik W, Fikre J, Sekuler R. Improvement in direction discrimination: No role for eye movements. *Percept Psychophys*. 1985;38:554–558.
53. Kosnik W, Kline D, Fikre J, Sekuler R. Ocular fixation control as a function of age and exposure duration. *Psychol Aging*. 1987;2:302–305.
54. Curcio CA, Allen KA. Topography of ganglion cells in human retina. *J Comp Neurol*. 1990;300:5–25.
55. Diaz-Santana L, Torti C, Munro I, Gasson P, Dainty C. Benefit of higher closed-loop bandwidths in ocular adaptive optics. *Opt Express*. 2003;11:2597–2605.
56. Hofer H, Artal P, Singer B, Aragon JL, Williams DR. Dynamics of the eye's wave aberration. *J Opt Soc Am A Opt Image Sci Vis*. 2001;18:497–506.
57. Mira-Agudelo A, Lundstrom L, Artal P. Temporal dynamics of ocular aberrations: Monocular vs binocular vision. *Ophthal Physiol Optics*. 2009;29:256–263.
58. Nirmaier T, Pudasaini G, Bille J. Very fast wavefront measurements at the human eye with a custom cmos-based hartmann-shack sensor. *Opt Express*. 2003;11:2704–2716.
59. Yu Y, Zhang Y. Dual-thread parallel control strategy for ophthalmic adaptive optics. *Chin Opt Lett*. 2014;12:121202. [PubMed].
60. Curcio CA, Owsley C. Rod-mediated dark adaptation as a suitable outcome for early and intermediate age-related macular degeneration. *Ophthalmology*. 2019;126:866–867.
61. Scoles D, Sulai YN, Cooper RF, et al. Photoreceptor inner segment morphology in best vitelliform macular dystrophy. *Retina*. 2017;37:741–748. [PubMed].
62. Owsley C, McGwin G, Jr., Searcey K. A population-based examination of the visual and ophthalmological characteristics of licensed drivers aged 70 and older. *J Gerontol A Biol Sci Med Sci*. 2013;68:567–573. [PubMed].
63. Chylack LT, Jr, Wolfe JK, Singer DM, et al. The lens opacities classification system iii. *Arch Ophthalmol*. 1993;111:831–836.